



EPTT-2020-0076

**INVESTIGATION OF TURBULENCE EFFECTS ON THE RISK OF
RUPTURE OF A MIDDLE CEREBRAL ARTERY ANEURYSM VIA CFD**

Cristian Ricardo Schwatz

Ricardo Nava de Sousa

Fluid Dynamics Laboratory, University of Blumenau
Rua São Paulo, 3250, I-204 – 89030-000 – Blumenau – Santa Catarina – Brazil
cristianrs@hotmail.com
ricardo.nava.sousa@gmail.com

Leandro José Haas

Health Sciences Department, University of Blumenau
Rua Antônio da Veiga, 140 – 89030-903 – Blumenau – Santa Catarina – Brazil
Hemodynamics, Santa Isabel Hospital
Rua Marechal Floriano Peixoto, 300 – 89010-906 – Blumenau – Santa Catarina – Brazil
ljhaas@terra.com.br

Christine Fredel Boos

Fluid Dynamics Laboratory, University of Blumenau
cfboos@gmail.com

Leonardo Machado da Rosa

Fluid Dynamics Laboratory, University of Blumenau
leorosa@gmail.com

Marcela Kotsuka da Silva

Fluid Dynamics Laboratory, University of Blumenau
marcelaks@gmail.com

Henry França Meier

Fluid Dynamics Laboratory, University of Blumenau
meier@furb.br

Jaci Carlo Schramm Câmara Bastos

Fluid Dynamics Laboratory, University of Blumenau
camarabastos@gmail.com

Abstract. *Aneurysms are diseases that affect a considerable part of the world population, which can present high mortality rates. Furthermore, they are asymptomatic, hindering its identification by the physician. Additionally, physicians adopt a methodology based on the aneurysm size in order to opt for surgical intervention. Hence, aneurysm identification and the evaluation of its rupture risk can aid the medical field. With this in mind, Computational Fluid Dynamics (CFD) tools were developed with the purpose of providing physicians with additional analysis parameters. Wall Shear Stress based parameters, such as the Time Average Wall Shear Stress (TAWSS), Oscillatory Shear Index (OSI), and Relative Residence Time (RRT) are some of the parameters often utilized to assess the risk of aneurysm rupture, as well as the risk of atherosclerotic plaque formation at the vessel wall. However, CFD-based tools are dependent on the numerical setup chosen, and thus, considerations such as which boundary conditions to use or whether turbulence modeling is considered, are of vital importance to the responsible for the numerical simulations. Thus, the present work has the objective of investigating the influence of a turbulence model over the risk of rupture of a middle cerebral artery aneurysm by evaluating Wall Shear Stress based parameters. In order to perform this assessment, a comparison among simulations that considered turbulence and a simulation that used a laminar approach was carried out. Additionally, a pulsatile inlet boundary condition was utilized, to closely model the physiological phenomena and the geometry used was reconstructed based on medical data.*

Keywords: *Hemodynamics, Intracranial Aneurysms, Turbulence, Rupture Risk, Computational Fluid Dynamics*

1. INTRODUCTION

Hemodynamics are believed to play a major role in the risk of atherosclerotic plaque formation and progression at artery walls. Additionally, atherothrombosis which may occur due to plaque presence, is one of the leading death and disability causes in the globe (KOCK et al., 2008). The formation of this plaque can also lead to the initiation of an aneurysm, which is a local dilatation of the arterial wall. It is known that worldwide, 2% to 5% of the population carries one or more aneurysms (BERNARDINI et al., 2011), which are often located at arterial bifurcations and curvatures (CASTRO et al., 2009). Due to this fact, cerebral aneurysms have a tendency to occur at the circle of Willis. Given this location, aneurysm rupture can lead to subarachnoid hemorrhage (SIGNORELLI et al., 2018), which can present death rates of up to 50% (BERNARDINI et al., 2011). Moreover, in cases where the patient survives, the rupture may cause morbidity. Hence, aneurysm rupture prediction can be of aid to physicians, since this clinical condition is able to remain asymptomatic until its rupture.

In order to assess this risk, Wall Shear Stress (WSS) based parameters can be calculated, such as the Time Averaged Wall Shear Stress (TAWSS), Oscillatory Shear Index (OSI) and Relative Residence Time (RRT). Such parameters are obtained with the use of Computational Fluid Dynamics (CFD) based tools and can be used alongside medical imaging techniques, such as MRI and CT-Scans. Nevertheless, when conducting CFD-based simulations, the phenomena behind blood flow, such as its rheology or turbulence, have a significant importance, in order to increase the simulation accuracy. Although both phenomena have a major role in blood flow, the former is often more focused in CFD studies. Despite presenting a shear-thinning behavior (RAZAVI; SHIRANI; SADEGHI, 2011), it was seen in past works that a Newtonian approach may yield reasonable results (KARIMI et al., 2014). Additionally, Jain, Roller and Mardal (2016) state that the transition Reynolds number for intracranial aneurysms is of the order of 500. Even though blood flow is known for presenting low Reynolds numbers, values higher than 500 can be encountered in an Internal Carotid Artery (ICA) (CEBRAL et al., 2009). Since the Middle Cerebral Artery (MCA) presents lower internal diameters than the ICA, it can yield higher Reynolds numbers, and thus, achieve transitional flow. Therefore, this work will be focusing on studying the influence of a turbulence model over the hemodynamic parameters in a middle cerebral artery aneurysm.

2. MATHEMATICAL MODELLING

2.1 GOVERNING EQUATIONS

From the time-dependent Navier-Stokes equation, the momentum balance can be written as Eq. (1), which yields the blood flow:

$$\frac{\partial}{\partial t} \rho \mathbf{u} = -[\nabla \cdot \rho \mathbf{u} \mathbf{u}] - \nabla p - [\nabla \cdot \boldsymbol{\tau}] \quad (1)$$

where ρ indicates the density of the fluid, \mathbf{u} the velocity vector, t the time, p the hydrostatic pressure and $\boldsymbol{\tau}$ the shear stress. Moreover, since blood can be taken as being incompressible, the continuity Eq. (2) is used:

$$[\nabla \cdot \mathbf{u}] = 0 \quad (2)$$

The shear stress in equation (1) is expressed using a Newtonian approach in Eq. (3):

$$\boldsymbol{\tau} = -\mu[\nabla \mathbf{u} + (\nabla \mathbf{u})^T] - \frac{2}{3}(\nabla \cdot \mathbf{u})\mathbf{I} \quad (3)$$

where μ denotes the dynamic viscosity of the fluid, $(\nabla \mathbf{u})^T$ the transpose of $\nabla \mathbf{u}$ and \mathbf{I} the identity tensor.

2.2 TURBULENCE MODELLING

In order to properly model the turbulence, Eq. (4) to Eq. (6) are averaged using the RANS approach:

$$\frac{\partial}{\partial t} [\rho \bar{\mathbf{u}}] + [\nabla \cdot \rho \overline{\mathbf{u} \mathbf{u}}] = -\nabla \bar{p} + [\nabla \cdot (\boldsymbol{\tau} - \rho \overline{\mathbf{u}' \mathbf{u}'})] \quad (4)$$

$$[\nabla \cdot \rho \bar{\mathbf{u}}] = 0 \quad (5)$$

$$-\rho \overline{\mathbf{u}' \mathbf{u}'} = \boldsymbol{\tau}^R \quad (6)$$

where the bar superscript denotes the time average, the apostrophe indicates fluctuations components and the new term at the right hand side of the equation is defined as the Reynolds Stress Tensor.

This tensor can be further expressed as Eq. (7), after applying the Boussinesq hypothesis:

$$\boldsymbol{\tau}^R = \mu_t [\nabla \mathbf{u} + (\nabla \mathbf{u})^T] - \frac{2}{3} \rho k \mathbf{I} \quad (7)$$

where μ_t represents the turbulent viscosity and k the turbulent kinetic energy, which can be defined according to Eq. (8) and Eq. (9), respectively:

$$\mu_t = \frac{c_\mu k^2}{\varepsilon} \quad (8)$$

$$k = \frac{1}{2} \overline{\mathbf{u}' \cdot \mathbf{u}'} \quad (9)$$

In this work, the k- ε model was utilized, in order to assess its impact over the hemodynamics of a MCA aneurysm. The two-equation model is expressed in Eq. (9) and Eq. (10):

$$\frac{\partial}{\partial t} [\rho k] + [\nabla \cdot \rho \mathbf{u} k] = \nabla \cdot (\mu_{eff,k} \nabla k) + P_k + \rho \varepsilon \quad (10)$$

$$\frac{\partial}{\partial t} [\rho \varepsilon] + [\nabla \cdot \rho \mathbf{u} \varepsilon] = \nabla \cdot (\mu_{eff,\varepsilon} \nabla \varepsilon) + C_{\varepsilon 1} P_k - C_{\varepsilon 2} \rho \frac{\varepsilon^2}{k} \quad (11)$$

where μ_{eff} is the effective viscosity, defined in Eq. (12), and ε is the rate of turbulence kinetic energy dissipation.

$$\mu_{eff,k} = \mu + \frac{\mu_t}{\sigma_k}; \quad \mu_{eff,\varepsilon} = \mu + \frac{\mu_t}{\sigma_\varepsilon} \quad (12)$$

Moreover, the constants are displayed in Eq. (13):

$$C_{\varepsilon 1} = 1.44, C_{\varepsilon 2} = 1.92, C_\mu = 0.09, \sigma_k = 1.0 \text{ and } \sigma_\varepsilon = 1.3. \quad (13)$$

2.3 WALL SHEAR STRESS BASED PARAMETERS

Since WSS related parameters are often linked to endothelial damage, these are required to be quantified, enabling its assessment. Amongst the known parameters, the Oscillatory Shear Index (OSI) and the Relative Residence Time (RRT) are believed to be related to atherosclerotic plaque formation (HE; KU, 1996), as well as with aneurysm rupture (LI et al., 2018). Soulis et al. (2011) describe that atherosclerotic sites have a tendency to present slower and disturbed flows, in which such disturbed flows can be determined by WSS related parameters.

The OSI is defined as being the cyclic oscillation of the WSS from its original vector direction, at time equals to zero (HE; KU, 1996), and can be defined according to Eq. (14):

$$OSI = \frac{1}{2} \left(1 - \frac{|\int_0^T \mathbf{WSS} dt|}{|\int_0^T \mathbf{WSS} dt|} \right) \quad (14)$$

where T is the duration of a cardiac cycle and \mathbf{WSS} is the instantaneous WSS vector. The numerator and denominator of Eq. (14) are defined as Time Averaged WSS vector and Time Averaged WSS, respectively:

$$TAWSSV = \frac{1}{T} \int_0^T |\mathbf{WSS} dt| \quad (15)$$

$$TAWSS = \frac{1}{T} \int_0^T |\mathbf{WSS}| dt \quad (16)$$

The quantification of the TAWSS has also a significant importance, as values higher than 40Pa can lead to endothelial damage and consequently increase the chance of thrombosis development (DONG; INTHAVONG; TU, 2013). Additionally, equation Eq. (14) shows that the OSI can vary from 0, for cases in which the WSS vector presented no variation during a cardiac cycle, up to 0.5, for cases that presented a 180° deflection of the WSS vector.

Lastly, the RRT is defined by the time a particle remains inside the domain, relative to the time it remains in a specific pre-determined region. Hence, this parameter is able to indicate flow stagnation (XU et al., 2018). (SOULIS et al., 2011) describe that high RRT regions may indicate a tendency of presenting the concentration of atheroma, which can consequently lead to atherosclerosis. The RRT is described in Eq. (16):

$$RRT = [(1 - 2 \times OSI) \times TAWSS]^{-1} \quad (16)$$

In this study, each RRT value was compared to the volume average value, which resulted in normalized values. This procedure was described in Peiffer, Sherwin and Weinberg (2013):

$$RRT_{normalized} = \frac{RRT}{RRT_{volume\ average}} \quad (17)$$

Although these parameters aid in the assessment of aneurysm rupture risk and possible vessel damage risk, the analysis provided by them is mainly qualitative, since these risks are not quantified.

3. MATERIALS AND METHODS

3.1 GEOMETRY RECONSTRUCTION

With the purpose of reconstructing an artery, real patient data was acquired from a 66 year old female that presented a saccular aneurysm at the bifurcation of her right middle cerebral artery (RMCA). Furthermore, all other patient data is unknown, with the aim of preserving her anonymity. This data was provided to us by the Santa Isabel Hospital, located in Blumenau, Brazil.

To obtain the data, an angio CT-Scan with the use of contrast was performed on the patient. Since a CT-Scan exam provides two-dimensional planes in three different views, a 3D model could be reconstructed by doing a superposition of such planes, which results in the formation of a three dimensional volume. This process is expressed in Fig. 1:

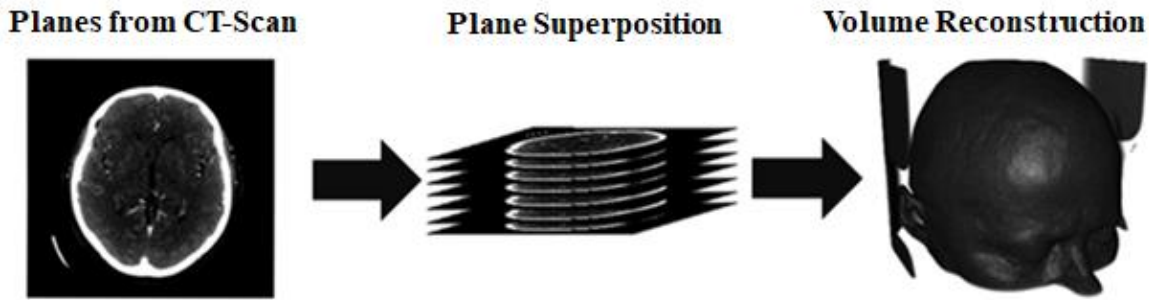


Figure 1. Generation of a three-dimensional volume from two dimensional scans from a CT-Scan.

In order to reconstruct the arterial system from the CT-Scans, the Open Source software package 3D Slicer was utilized. Additionally, alongside the software, the SlicerVMTK extension was used, which has the purpose of providing tools for vascular reconstruction, as 3D slicer presents difficulties when reconstructing blood vessels with smaller diameters. In the first step of the reconstruction, the arterial tree is built, as shown in Fig. 2:



Figure 2. Reconstructed head blood vessels.

It is possible to see in Fig. 2 that the software captures all possible entities with similar contrast level, leading to the creation of a complex three-dimensional geometry. Moreover, the software also reconstructs possible noise captured in the CT-Scan machine. Therefore, after generating the first geometry, a manual segmentation was performed, to remove all entities that are not of interest and to reduce the size of the geometrical domain, easing the computational requirement by the numerical simulation. It is important to notice that, since segmentation was performed manually, the quality of the geometrical domain is directly affected by the software operator, which may have an influence over the obtained results. Once the segmentation was performed, the RMCA, as well as the aneurysm geometries were obtained, as seen in Fig. 3:



Figure 3. RMCA reconstruction after manual segmentation.

The last step of the geometry reconstruction was to export the model as a .stl format, which is supported by ANSYS ICEM v15, as it was the software used in the numerical mesh generation. Moreover, extensions were created at the inlet and all the outlets of the geometry, in order to have a fully developed flow at the inlet and to avoid outlet boundary conditions effects on the outlets. The extensions are represented in Fig. 4:

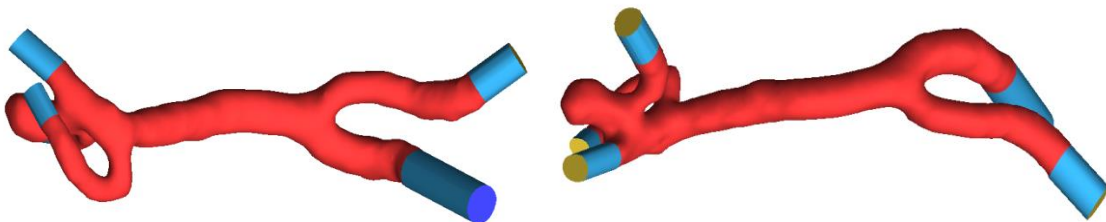


Figure 4. Anterior and Posterior views of the reconstructed RMCA.

3.2 NUMERICAL MESH

With the purpose of discretizing the spatial domain and solve the conservation equations, a numerical mesh was developed. Similarly to the extensions, the numerical mesh was generated in the ANSYS ICEM v15 software. For this geometry, three tetrahedral meshes were constructed using the OCTREE method. This choice is justified by the irregularity and complexity presented in the present geometrical domain. Furthermore, a prism layer was developed at the wall region to increase wall phenomena accuracy. Additionally, the maximum element size defined for this mesh was 0.2mm, as proposed by Ou et al. (2016). In order to closely match the element size, the prism layer contained a total height of 0.19mm, with four layers that have a growth ratio as the elements are further away from the wall. The three meshes created were divided into coarse, intermediate and refined meshes, with the aim of carrying out the Grid Convergence Index (GCI), as described by Celik et al. (2008). Once the GCI was carried out, the intermediate mesh was chosen, as the numerical error arisen from the mesh was in an acceptable range. The chosen numerical mesh contains 314 thousand elements and is showed in Fig. 5:

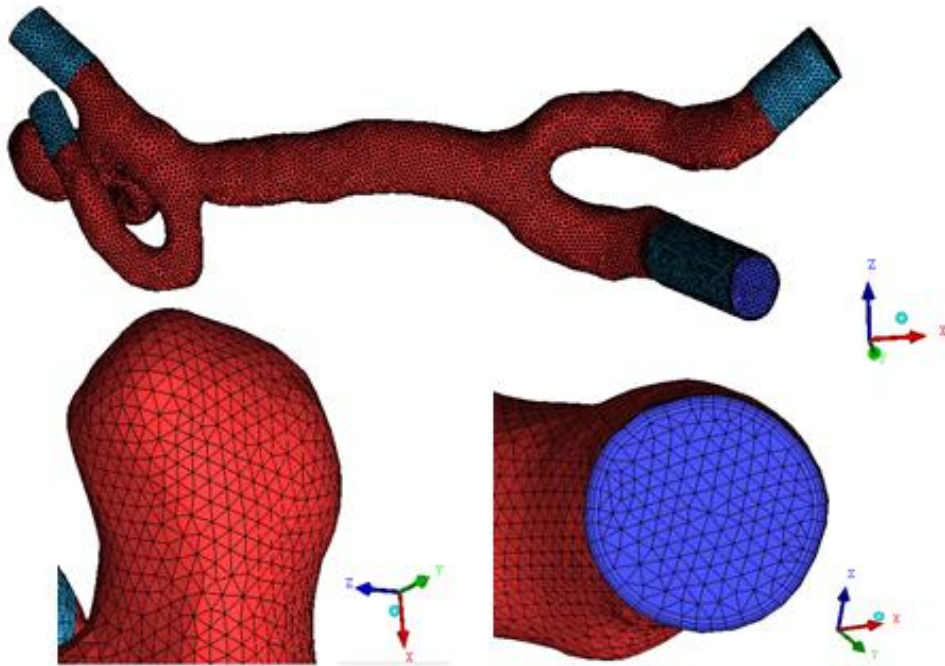


Figure 5. Numerical mesh of the RMCA.

3.3 NUMERICAL SETUP

In order to carry out the simulations with an acceptable accuracy, proper boundary conditions and parameters have to be set. Regarding the boundary conditions, the artery walls were taken to be rigid, and thus, a no-slip boundary condition was applied. A prescribed pressure boundary condition was used at the outlets, and pressure was taken to be constant at an average physiological level of 100mmHg. At the inlets, a pulsatile flow boundary condition was applied. In order to obtain a pulsatile function for this condition, the studies of Watanabe (2013) were utilized to obtain a blood flow rate function at the MCA, as shown in Fig. 6:

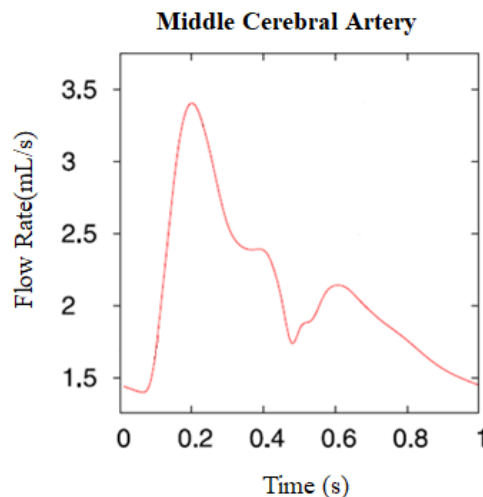


Figure 6. Blood flow rate in a MCA during a cardiac cycle.

The data was then extrapolated and exported to the Matlab software, in which an 8th order Fourier regression was carried out, which resulted in eighteen coefficients with a 95% confidence bound and a R-square over 0.99. This regression made use of Eq. (17):

$$y = a_0 + \sum_{i=1}^n a_i \cos(iwx) + b_i \sin(iwx) \quad (17)$$

where a_0 models a constant term for $i = 0$ in the cosine term, w is defined as the fundamental frequency of the signal and n is the number of harmonics in the series, which can vary from 1 to 8. Additionally, the obtained function was utilized to write an User Defined Function (UDF) to enable its adoption as the inlet boundary condition. The resulting cyclic pulsatile function is presented in Fig. 7:

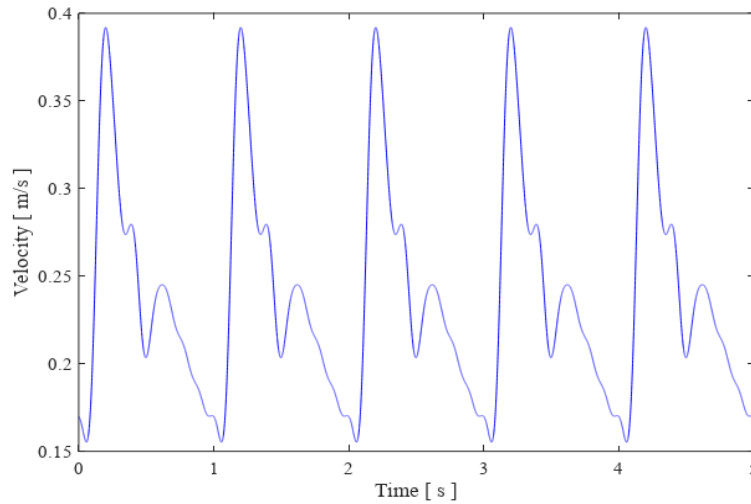


Figure 7. Pulsatile inlet velocity function for the MCA.

With the objective of presenting the values of constants and parameters, as well as the boundary conditions chosen in both simulations, this data is summarized in Tab. 1:

Table 1. Solver parameters and boundary conditions.

Parameters and Boundary Conditions	Setup Chosen
Blood Density	$\rho_{blood} = 1050kg/m^3$
Blood Newtonian Viscosity	$\mu_{Blood} = 0.004Pa.s$
Rheological Model	Newtonian
Turbulence Model	None / k- ϵ model
Inlet Boundary Condition	Pulsatile Velocity (UDF)
Outlets Boundary Conditions	$\overline{P_{blood}} = 100mmHg$
Wall Boundary Condition	No-slip velocity
Time step	10^{-4}

The values presented in Tab. 1 were taken from the studies of Schwatz et al. (2019). It is important to point out that two simulations were carried out, and the only difference between them was the usage of the k- ϵ turbulence model. Lastly, 5s of simulation were carried out in both cases and the first 4s were discarded, in order to guarantee a pseudo-stationary condition.

4. RESULTS AND DISCUSSION

4.1 WALL SHEAR STRESS BASED PARAMETERS

The proposed simulations were carried out according to the setup described in the previous section and are presented in this section.

The first parameter analyzed was the TAWSS, in which an average value was quantified over an entire cardiac cycle. Its relevancy is justified by the fact that abnormally high TAWSS values are correlated to endothelial damage,

increasing the risk of a thrombosis (DONG; INTHAVONG; TU, 2013), or ischemic stroke, in cases of atherosclerotic plaque presence (DONG; WONG; TU, 2013). The computed TAWSS for both cases is presented in Fig. 8 and Fig. 9:

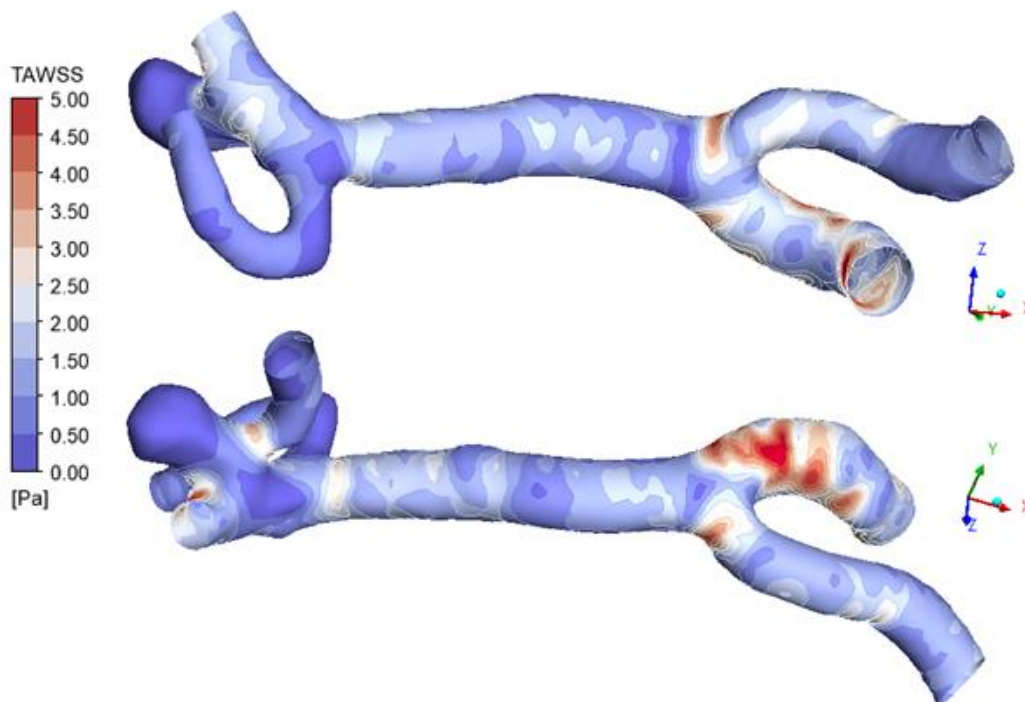


Figure 8. TAWSS of the anterior and posterior views of the RMCA for the model without a turbulence model.

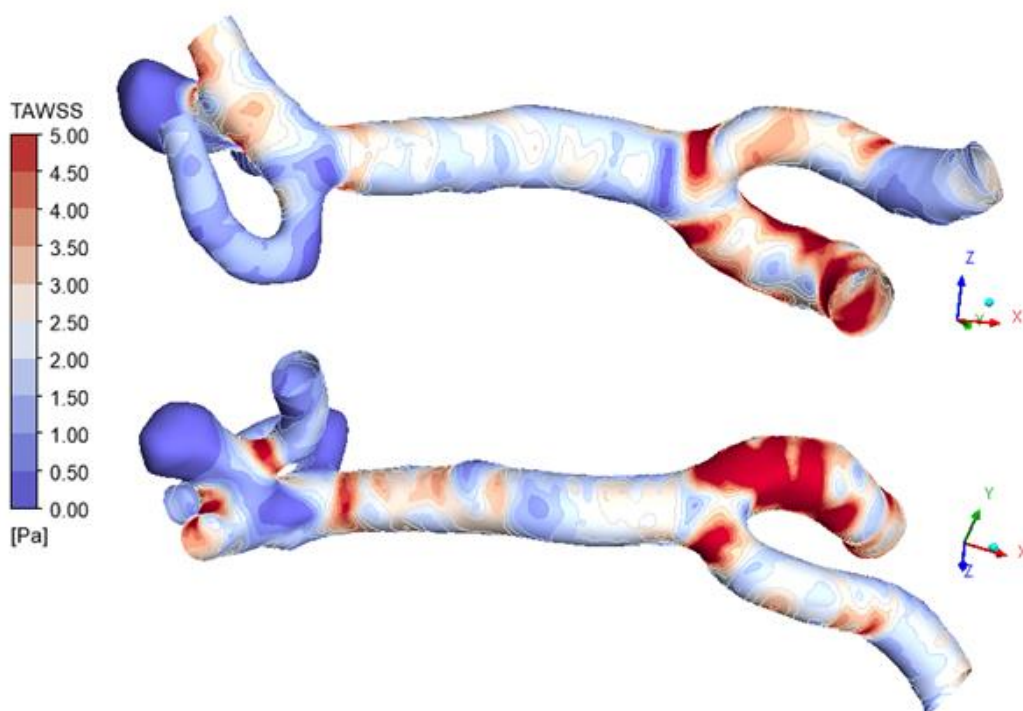


Figure 9. TAWSS of the anterior and posterior views of the RMCA for the model with the adoption of a turbulence model.

From Fig. 8 and Fig. 9 it can be observed that, qualitatively, TAWSS values are higher for the case which adopted the $k-\epsilon$ model. Moreover, the regions with the highest observed WSS were at the posterior region of the ICA and at arterial bifurcations. Knowing that arterial bifurcations are more susceptible to atherosclerotic plaque formation (DONG; INTHAVONG; TU, 2013; SKIADOPOULOS; NEOFYTOU; HOUSIADAS, 2017), the higher values of TAWSS at the bifurcations are in accordance with the literature, since higher values increase the risk of vessel damage. On the other hand, the aneurysm region presented the lowest TAWSS values. Since this region yields lower flow

velocities and that WSS is a function of shear rate, such values of TAWSS can be expected. Nevertheless, low WSS values increase cell permeability, promoting inflammatory cell infiltration, consequently increasing endothelial vulnerability (SKIADOPOULOS; NEOFYTOU; HOUSIADAS, 2017). Furthermore, lower WSS or TAWSS ranges may increase the risk of aneurysm rupture (SHAMLOO; NEJAD; SAEEDI, 2017).

4.2 OSCILLATORY SHEAR INDEX

In addition to the TAWSS, the OSI was also quantified, as this parameter also aids in the assessment of aneurysm rupture and vessel damage risks. This is due to the correlation of high OSI values with the increase of aneurysm growth and rupture risk (SHAMLOO; NEJAD; SAEEDI, 2017). The OSI contours are presented in Fig. 10 and Fig. 11:

Fig. 10 and Fig. 11 indicate that, qualitatively, despite visible similarities, the case with the adoption of a turbulence model yielded higher OSI values. Knowing that the latter case also showed higher TAWSS, higher OSI values were to be expected, as TAWSS is the denominator in Eq. (14). Furthermore, OSI represents the oscillatory behavior of the flow during a cardiac cycle, and thus, by using a turbulence model, this behavior can be more accurately captured. Additionally, both figures show that the regions that display high OSI values are arterial bifurcations and the aneurysm dome, which are the regions with the tendency of suffering damage from these hemodynamic forces (HE; KU, 1996).

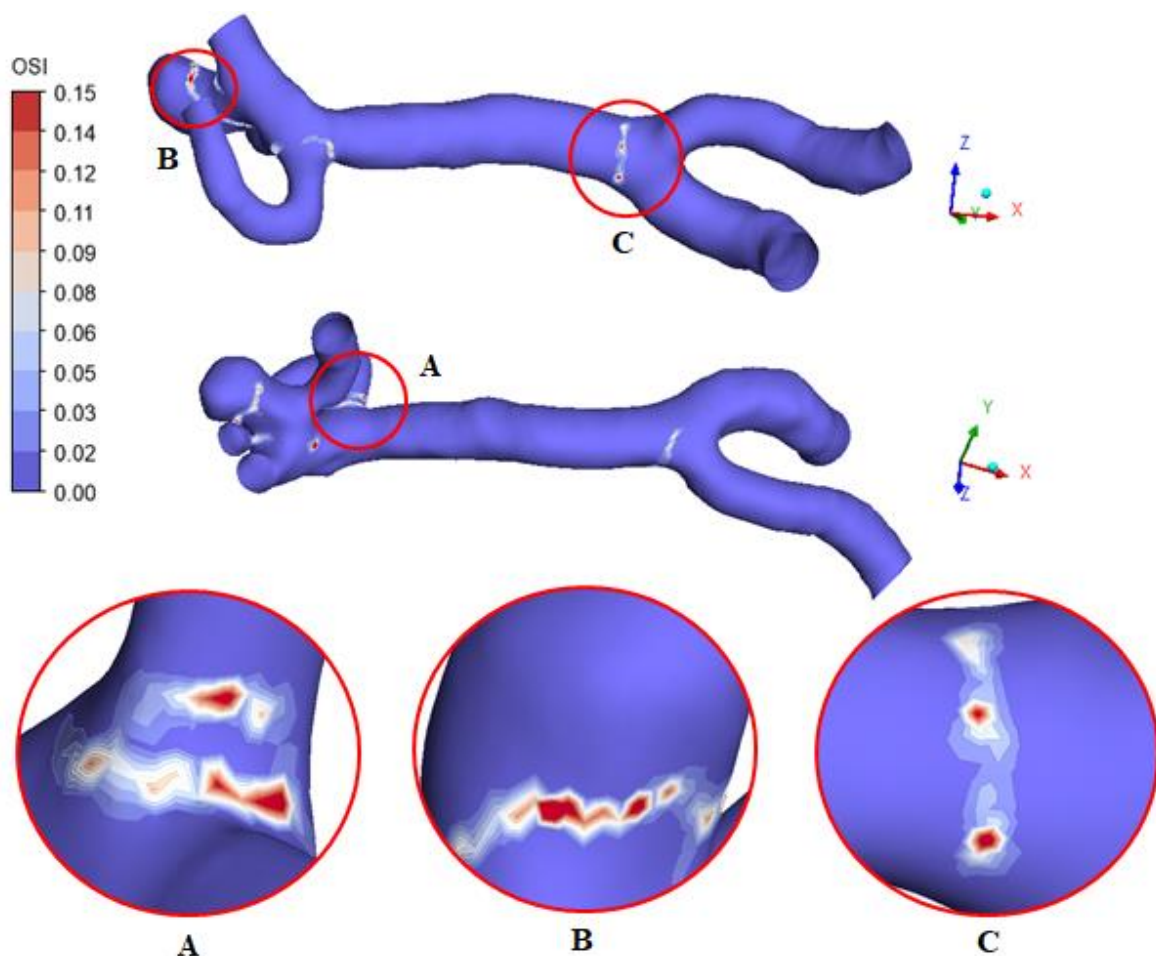


Figure 10. OSI contours for the anterior and posterior views of the RMCA and highlighted regions for the case without turbulence modelling.

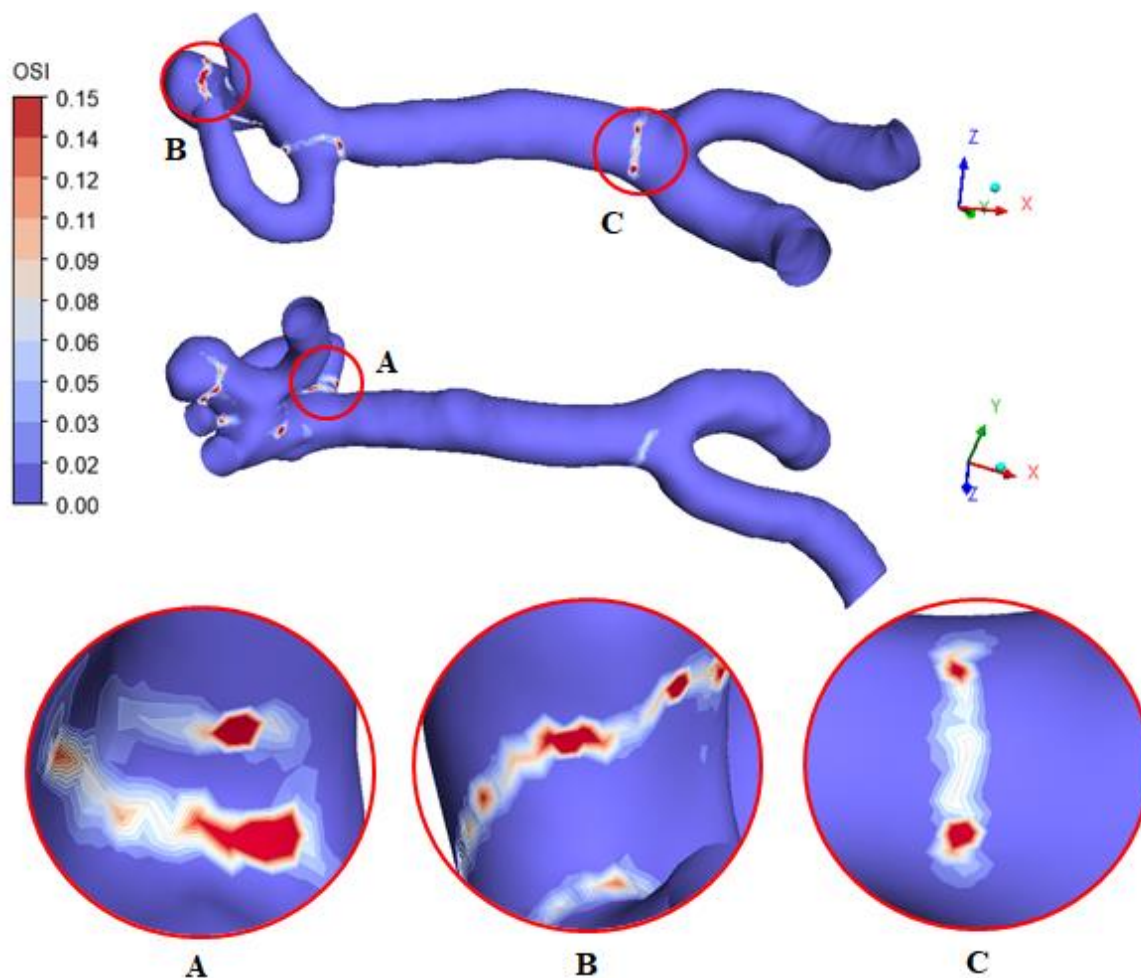


Figure 11. OSI contours for the anterior and posterior views of the RMCA and highlighted regions for the case with the adoption of a turbulence model.

4.3 RELATIVE RESIDENCE TIME

Lastly, the RRT was also quantified with the aim of providing further aneurysm rupture and vessel damage risk assessment. Similarly to the OSI, high RRT values indicate higher probability of aneurysm rupture, since it is linked to blood flow stagnation (LI et al., 2018). The RRT contours are displayed in Fig. 12 and Fig. 13. From these figures it can be seen that the RRT also followed the trend of yielding higher values for the case with the adoption of a turbulence model. Furthermore, Fig. 12 and Fig. 13 show that the aneurysm domes are the main region with high RRT values. These high values can be possibly explained by the stagnation caused due to the concentration of circulatory flow inside the aneurysm, as well as to the deceleration suffered by the blood when entering the aneurysm dome. Moreover, when comparing Fig. 10 and 11 with Fig. 12 and Fig. 13, it becomes visible that the areas with the highest OSI values are similar to those with the highest RRT values.

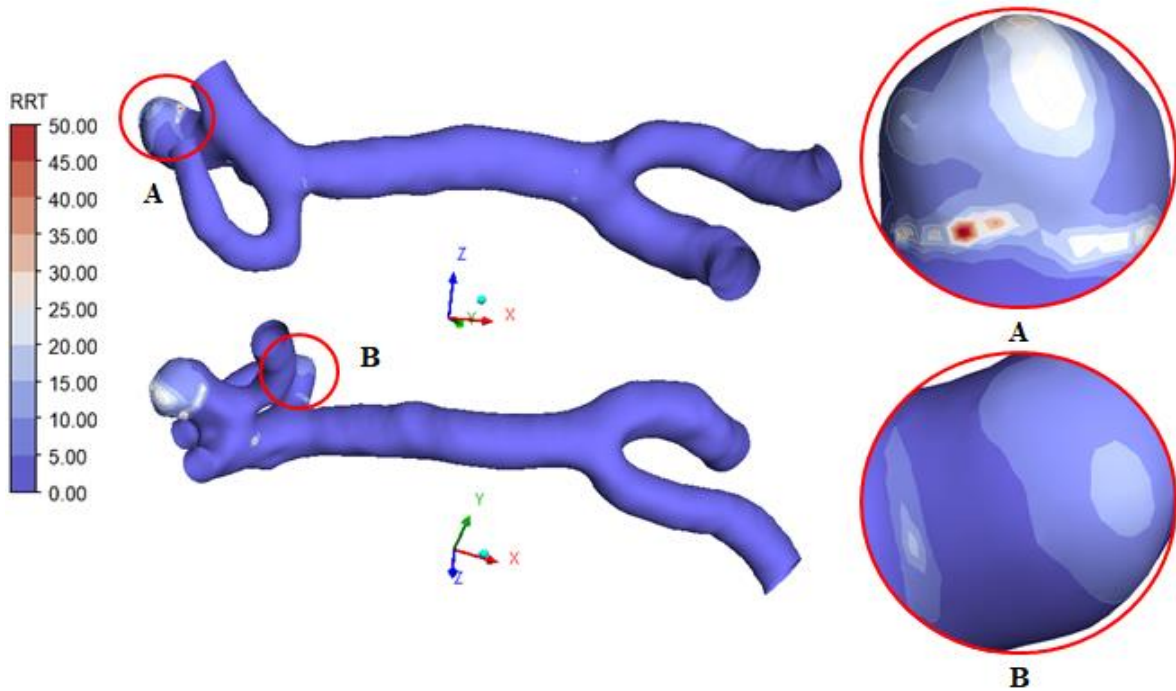


Figure 12. RRT contours for the anterior and posterior views of the RMCA and highlighted regions for the case with the adoption of a turbulence model.

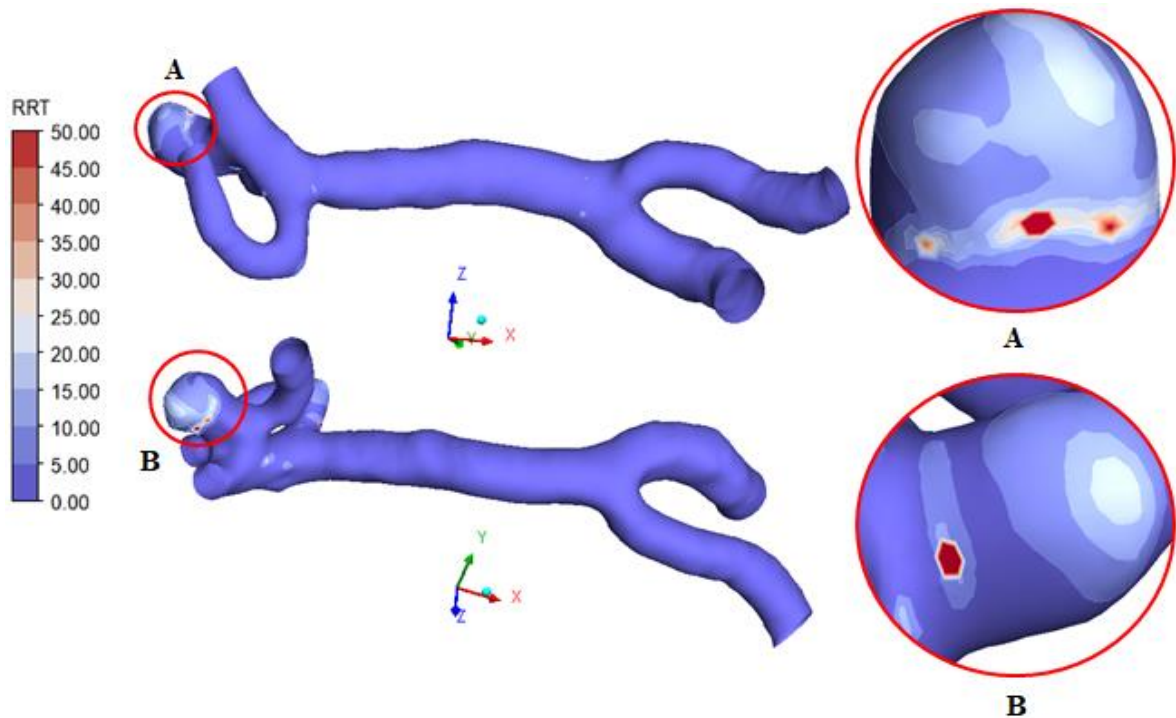


Figure 13. RRT contours for the anterior and posterior views of the RMCA and highlighted regions for the case with the adoption of a turbulence model.

4.4 VELOCITY STREAMLINES AND QUANTITATIVE RESULTS

In addition to the color maps for the WSS-based parameters, their maximum values were also quantified to provide further comparison and are presented in Tab. 2. From the results computed in Tab. 2 it is possible to see that all parameters in the $k-\epsilon$ model presented higher values, which were discussed in their respective sections. Furthermore, this data indicates that by considering the usage of a turbulence model, WSS-based parameters might be overestimated, or that a laminar approach might cause the opposite.

The velocity streamlines were also analyzed, which can be seen in Figure 14. In order to analyze the streamlines over a full cardiac cycle, it was decided to divide it into five different time steps, covering both the systole and the diastole phase of the cardiac cycle. These phases correspond to the contraction and relaxation of the heart, respectively. The systole is represented by the peak in the most left image of Figure 14, whereas the diastole is represented by the furthest right image in Figure 14. Disturbed flows were observed in both cases, in which they became more chaotic during the systolic phase. Moreover, the presence of intra-aneurysm vortexes was also noticed. Despite qualitative results showing a supposedly higher oscillatory behavior in the laminar case, especially at the third image from left to right, the results from Tab. 2 indicate that the $k-\epsilon$ model has, in fact, a higher oscillatory behavior. This can be justified by the fact that the case with the turbulence model does consider the presence of eddies and their impact over the flow. Additionally, higher velocities were encountered in the laminar case, which justify the lower RRT values presented by this case.

Table 2. Maximum TAWSS, OSI and RRT values for both cases.

CASE	TAWSS _{max} (Pa)	OSI _{max}	RRT _{max}
Laminar	7.4464	0.38206	60.4515
$k-\epsilon$ model	13.5663	0.4568	137.0910

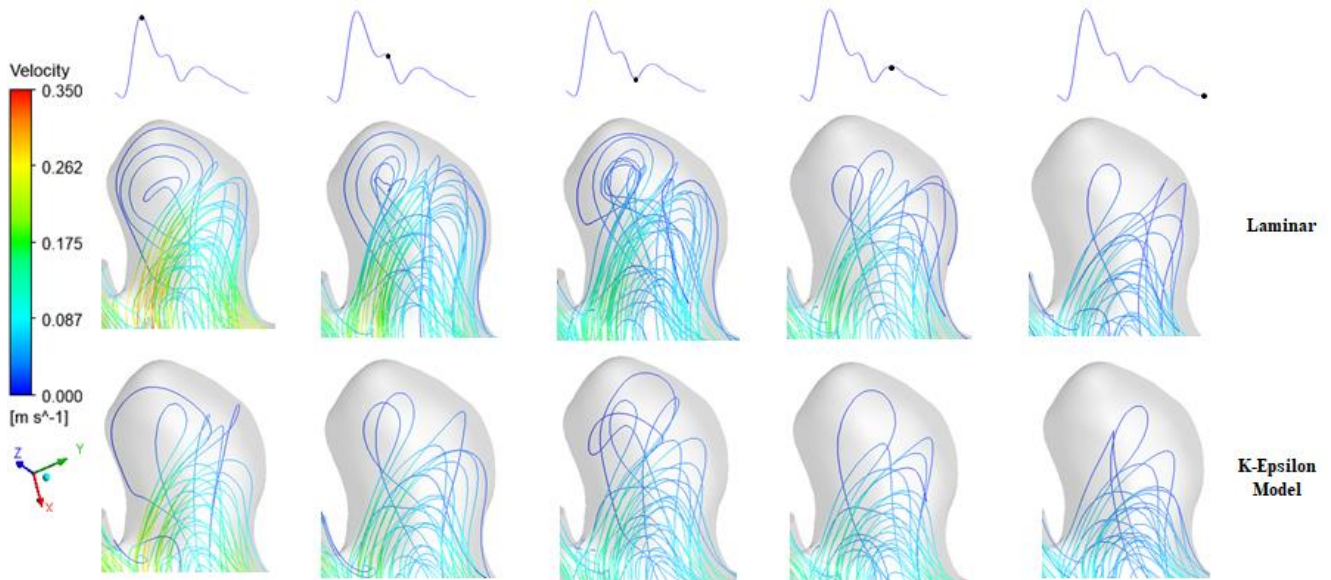


Figure 14. Velocity streamlines inside the aneurysm for both models.

5. CONCLUSIONS

With the aid of CFD-based tools, the influence of a turbulence model over hemodynamic parameters in a middle cerebral artery was studied. Additionally, an assessment of the risk of aneurysm rupture and vessel damage was made. From the results presented in the previous section, the conclusions that could be drawn are:

- TAWSS results showed that lower values were encountered at the aneurysm dome region, which can increase cell permeability and consequently increase the chance of aneurysm rupture. High TAWSS values were observed at arterial bifurcations, such as the ICA bifurcation and the MCA bifurcation, which are correlated to endothelial damage and atherosclerotic plaque formation and growth. Moreover, the usage of the $k-\epsilon$ model increased TAWSS values;
- OSI presented its highest values at the aneurysm dome and at the bifurcations of the artery. Such values were even higher when the $k-\epsilon$ model was considered, which might be due to the increase in oscillatory behavior of the flow;
- Differently from the other parameters, the RRT only had significantly high values at the aneurysm dome. However these values are often linked to aneurysm rupture. Furthermore, following the trend of the other parameters, RRT values were significantly higher when adopting the $k-\epsilon$ model;
- Lower velocities were observed when using the turbulence model, which consequently impacts all other hemodynamic parameters. Thus, the consideration of using a turbulence model may overestimate WSS-

based parameters, due to an increased oscillatory behavior of the flow. Nevertheless, it is necessary to further analyze turbulence models before any claims can be made.

6. ACKNOWLEDGEMENTS

The authors would like to acknowledge M.D. Leandro José Haas and the Santa Isabel Hospital for providing the patient data that was used in this work.

This study was financed in part by the Coordenação de Aperfeiçoamento de Pessoal de Nível Superior - Brasil (CAPES) - Finance Code 001.

7. REFERENCES

- BERNARDINI, A. et al. Influence of different computational approaches for stent deployment on cerebral aneurysm haemodynamics. *Interface Focus*, v. 1, n. 3, p. 338–348, 2011.
- CASTRO, M.; PTUMAN, C.M.; RADAELLI, A.; FRANGI, A.; CEBRAL, J.R. Hemodynamics and Rupture of Terminal Cerebral Aneurysms. *Academic Radiology*. 2009, 16, 1201-1207.
- CEBRAL, J. R.; PUMAN, C.M.; ALLEY, M.T.; HOPE, T.; BAMMER, R.; CALAMANTE, F. Hemodynamics in normal cerebral arteries: qualitative comparison of 4D phase-contrast magnetic resonance and image-based computational fluid dynamics. *Journal of Engineering Mathematics*. v. 64. p. 367–378, 2009.
- CELIK, I. B.; GHIA, U.; ROACHE, C. J.; FEITAS, C. J.; COLEMAN, H.; RAAD, P. E. Procedure for Estimation and Reporting of Uncertainty Due to Discretization in CFD Applications. *Journal of Fluid Engineering*, v. 130, n. July 2008, p. 1–4, 2008.
- DONG, J.; INTHAVONG, K.; TU, J. Image-based computational hemodynamics evaluation of atherosclerotic carotid bifurcation models. *Computers in Biology and Medicine*, v. 43, n. 10, p. 1353–1362, 2013.
- DONG, J.; WONG, K. K. L.; TU, J. Hemodynamics analysis of patient-specific carotid bifurcation : A CFD model of downstream peripheral vascular impedance. *International Journal for Numerical Methods in Biomedical Engineering*. John Wiley & Sons, n.29, p. 476–491, 2013.
- HE, X.; KU, D. N. Pulsatile Flow in the Human Left Coronary Artery Bifurcation : Average Conditions. v. 118, n.74, p. 74–82, 1996.
- JAIN, K.; ROLLER, S.; MARDAL, K. Transitional flow in intracranial aneurysms – A space and time refinement study below the Kolmogorov scales using Lattice Boltzmann Method. *Computers and Fluids*. v. 127, p. 36–46, 2016.
- KARIMI, S.; DABAGH, M.; VASAVA, P.; DADVAR, M.; DABIR, B.; JALALI, P. Effect of rheological models on the hemodynamics within human aorta: CFD study on CT image-based geometry. *Journal of Non-Newtonian Fluid Mechanics*. Elsevier, v. 207, p. 42–52, 2014.
- KOCK, S. A.; NYGAARD, J.V.; ELDRUP, E.; FRUND, E.; KLAERKE, A.; PAASKE, W.; FALK, E.; KIM, W.Y. Mechanical stresses in carotid plaques using MRI-based fluid-structure interaction models. *Journal of Biomechanics*, v. 41, n. 8, p. 1651–1658, 2008.
- LI, M.; WANG, J.; LIU, J.; ZHAO, C.; YANG, X. Hemodynamics in Ruptured Intracranial Aneurysms with Known Rupture Points. *World Neurosurgery*. p. 1–6, 2018.
- OU, C.; HUANG, W.; YUEN, M. M. F.; QIAN, Y. Hemodynamic modeling of leukocyte and erythrocyte transport and interactions in intracranial aneurysms by a multiphase approach. *Journal of Biomechanics*. Elsevier, v. 49, n. 14, p. 3476–3484, 2016.
- PEIFFER, V.; SHERWIN, S. J.; WEINBERG, P. D. Computation in the rabbit aorta of a new metric – the transverse wall shear stress – to quantify the multidirectional character of disturbed blood flow. *Journal of Biomechanics*, v. 46, n. 15, p. 2651–2658, 2013.
- RAZAVI, A.; SHIRANI, E.; SADEGHI, M. R. Numerical simulation of blood pulsatile flow in a stenosed carotid artery using different rheological models. *Journal of Biomechanics*, v. 44, n. 11, p. 2021–2030, 2011.
- SHAMLOO, A.; NEJAD, M. A.; SAEEDI, M. Fluid – structure interaction simulation of a cerebral aneurysm : Effects of endovascular coiling treatment and aneurysm wall thickening. *Journal of the Mechanical Behavior of Biomedical Materials*, v. 74, n. February, p. 72–83, 2017.
- SIGNORELLI, F.; SELA, S.; GESUALDO, L.; CHEVREL, S.; TOLLET, F.; PAILLER-MATTEI, C.; TACCONI, L.; TURJMAN, F.; VACCA, A.; SCHUL, D. B. Hemodynamic Stress, Inflammation, and Intracranial Aneurysm Development and Rupture: A Systematic Review. *World Neurosurgery*, v. 115, p. 234–244, 2018.
- SKIADOPOULOS, A.; NEOFYTOS, P.; HOUSIADAS, C. Comparison of blood rheological models in patient specific cardiovascular system simulations. *Journal of Hydrodynamics*, v. 29, n. 2, p. 293–304, 2017.
- SOULIS, J. V.; LAMPRI, O. P.; FYTANIDIS, D. K.; GIANNOGLOU, G. D. Relative Residence Time and Oscillatory Shear Index of Non-Newtonian Flow Models in Aorta. n. 1, p. 0–3, 2011.
- XU, L. et al. Flow instability detected in ruptured versus unruptured cerebral aneurysms at the internal carotid artery. *Journal of Biomechanics*, v. 72, p. 187–199, 2018.

8. RESPONSIBILITY NOTICE

This work was approved by the Brazilian Ethics Committee, which holds the process number 3.605.595, along with the CAAE 18146719.1.9999.5370, in order to fulfill legal requirements.

The authors are the only responsible for the printed material included in this paper.